Planetary and Space Science 155 (2018) 91–98

Contents lists available at ScienceDirect

Planetary and Space Science

journal homepage: www.elsevier.com/locate/pss

0.2 to 10 keV electrons interacting with water ice: Radiolysis, sputtering, and sublimation

A. Galli *, A. Vorburger, P. Wurz, A. Pommerol, R. Cerubini, B. Jost, O. Poch, M. Tulej, N. Thomas

Physikalisches Institut, University of Bern, Bern, Switzerland

ARTICLE INFO

Keywords:
Ices
Jupiter satellites
Experimental techniques
Sputtering

ABSTRACT

We present new laboratory experiments investigating various water ice samples, ranging from thin ice films to porous thick ice layers, that are irradiated with electrons. The molecules leaving the ice are monitored with a pressure gauge and a mass spectrometer. Most particles released from the ice are H_2 and O_2, the observed ratio of 2:1 is consistent with H_2O being radiolysed into $H_2 + 1/2\ O_2$ upon irradiation. H_2O_2 is likely a minor contribution of radiolysis, amounting to 0.001 ± 0.001 of the total gas release from the ice sample. Neither the physical properties of the ice, nor the energy, nor the electron impact angle have any obvious effect on the relative abundances of the radiolysis products. The absolute sputtering yield (i.e., the ratio of produced O_2 or destroyed H_2O per impacting electron) increases with energy until a few 100 eV. For higher energies up to 10 keV the yield remains roughly constant, once the saturation dose of the ice is reached. This indicates that ongoing irradiation eventually releases the radiolysis products from the water ice even for penetration depths of several micrometers.

1. Introduction

Electrons are part of every space plasma and of every ionosphere. Electron irradiation of icy surfaces therefore is an ubiquitous process in the outer Solar System for satellites and comets with tenuous atmospheres (for an overview of radiation effects on the surfaces of the Galilean moons see for instance Johnson et al. (2004)).

Whereas ion sputtering of water ice has often been studied in laboratory experiments (Haring et al. (1984); Reimann et al. (1984); Famá et al. (2008); Baragiola et al. (2008); Cassidy et al. (2013); Muntean et al. (2016); Galli et al. (2017) among others), the release processes of water ice irradiated with electrons has attracted less attention (Baragiola et al. (2002); Orlando and Sieger (2003), see Teolis et al. (2017) for a recent overview). To our knowledge, no experimental sputtering yields exist for electron energies above 100 eV except the few experiments described in Galli et al. (2017). There we found, for energies below 1 keV, the observed yield agreed with previous experiments (Orlando and Sieger, 2003) and theoretical expectations (Teolis et al., 2017). For 1 and 3 keV, however, the sputtering yield seemed to remain higher than expected. The major problem for interpretation was the penetration depth of energetic electrons. Because the experiments of Galli et al. (2017) had been performed only with thin ice films on a microbalance, the ice film was not thick enough to capture all electrons before they hit the metal underneath the ice.

We therefore expanded the latter experiments to a more comprehensive study of the interaction of electrons with water ice samples, ranging from 100 nm thin ice films to centimeter-thick porous or dense ice samples. We concentrated on the particles leaving the ice, measuring the quantity and the chemical composition of ejecta for the electron energy range between 200 eV and 10 keV. The laboratory experiments were performed at conditions typical for the icy moons of Jupiter since we wanted to verify the importance of electron precipitation relative to ion precipitation on icy moons: Galileo measurements of energetic electrons and ions upstream of Europa (Paranicas et al., 2001, 2002) showed that the energy flux of ions peaks between 100 and 1000 keV (Johnson et al., 2004), whereas the electron energy spectrum decreases with an almost constant power law from 10 keV to 10 MeV. The energy flux of electrons (4×10^{10} keV cm^{-2} s^{-1}) integrated from 10 keV to 200 MeV exceeds the one of the most common ion species H^+, O^+, and S^+ by factors of 5, 20, and 10, respectively. However, the sputtering yields of these ions in water ice reach their maxima between 100 keV and 10 MeV and are many orders of magnitude higher (Famá et al., 2008; Cassidy et al., 2013) than the sputtering yield predicted for electrons even at their most efficient energy of 0.4 keV (see next Section 2). As a result, we expected ion precipitation on Europa (and other icy moons inside the Jovian and Cronian magnetosphere) to dominate over electrons in terms of sputtering and atmospheric release processes. On the other hand,

* Corresponding author.
E-mail address: andre.galli@space.unibe.ch (A. Galli).

https://doi.org/10.1016/j.pss.2017.11.016
Received 19 April 2017; Received in revised form 16 November 2017; Accepted 22 November 2017
Available online 26 November 2017

electron precipitation dominates the energy deposition rate in the deeper ice layers (because of the different penetration depth) and likely determines the IR-absorption features of the surface (Paranicas et al., 2001). We plan to study the alteration of icy surfaces as a result of irradiation in future laboratory experiments. Here, we restrict ourselves to the study of released particles as a result of electron irradiation.

We will briefly summarize the expectations for water ice sputtering resulting from electrons (Section 2) and describe our ice sample preparation (Section 3.1) and our measurement methods (Section 3.2). The results will be presented in Section 4, followed by the conclusions in Section 5.

2. Theory

As energetic electrons impact in water ice, they deposit their kinetic energy in the form of electronic excitation of the water ice molecules. This triggers a chain of chemical reactions leading predominantly to the destruction of H_2O and the formation of H_2 and O_2. These radiolysis products diffuse from the ice directly or can be released by ongoing irradiation and destruction of the surface layers. Contrary to ion sputtering, H_2O molecules constitute only a minor fraction of the ejecta. This basic concept of water ice irradiation with electrons is based on previous experiments at low energies (see Johnson et al. (2013) and Teolis et al. (2017) for reviews). The ratio of the main radiolysis species H_2 and O_2 should be 2:1 once an equilibrium of production and release is reached (Teolis et al., 2009). A minor fraction of H_2O_2 was observed in previous irradiation experiments with ions and electrons (Hand and Carlson, 2011), and a spectroscopic feature of Europa's surface (Carlson et al., 1999) indicates a H_2O_2 concentration of 0.13% on Europa's surface (Loeffler et al., 2006). Johnson and Quickenden (1997) discussed in a more theoretical approach the production of the species H, H_2, O, OH, H_2O, H_3O, O_2, HO_2, H_2O_2, and their ions due to photolysis and radiolysis in water ice. For this study, we discuss only neutral species because we cannot detect positive or negative ions released from the ice.

Teolis et al. (2010, 2017) predicted the sputtering yield in terms of produced O_2 per impacting electron based on experiments (Baragiola et al., 2002; Boring et al., 1983; Orlando and Sieger, 2003) at low energies:

$$Y_{O2}(E,T,\theta) = \frac{E}{U_{O2}}\frac{x_0}{d\cos\theta} \times \left[1-\exp\left(-\frac{d\cos\theta}{x_0}\right)\right]\left(1+q_{O2}\exp\left(\frac{-E_d}{k_B T}\right)\right) \quad (1)$$

with $d\cos\theta$ the penetration depth, $x_0 = 2.8$ nm the thickness of the surface layer where O_2 production is efficient, $U_{O2} = 200$ eV at low temperatures, k_B the Boltzmann constant, and $q_{O2} = 1000\pm100$ the fit variable for the thermal dependence. This formula also fits the O_2 production caused by ions irradiating ice films at temperatures below 120 K (Teolis et al., 2010). The yield Y_{O_2} in Equation (1) increases linearly with energy but then turns over around 400 eV because the penetration depth becomes larger than the surface layer thickness x_0.

The penetration depth d of electrons in water ice can be approximated (Johnson, 1990; Hand and Carlson, 2011) by

$$d \approx R_0 E^{\alpha} \quad (2)$$

with E the electron energy in units of keV, $\alpha = 1.76$, and the depth $R_0 = 46$ nm for targets with density $\rho = 1$ g cm^{-3} at 1 keV. This density is realistic for compact ice films (see Section 3.1); we will discuss in the results if porosity influences the outcome.

Two issues that can complicate ice irradiation studies are surface charging (see for instance Shi et al. (2012) and Galli et al. (2016) for the case of ions) and surface heating effects. For experiments, irradiating ice with electrons has the benefit that fast electrons eject secondary electrons from the water ice. This secondary electron yield exceeds unity for energies between 0.05 and 10 keV (Jurac et al., 1995). This has the counter-intuitive effect that the ice surface is charged to a positive potential upon electron irradiation. The surface potential reaches values on the order of an eV (Jurac et al., 1995) and therefore is negligible compared to the electron energies of 0.2–10 keV we used.

Heating effects, on the other hand, can occur for thick ice samples and will lead to sublimation. For experiments at a given partial pressure of water, the water ice must be kept at a temperature below the sublimation temperature T_c (Andreas, 2007). If the electron flux on the ice surface is too strong the surface may heat up to a local temperature above T_c. If heat conduction between the regolith grains is neglected and only radiation applies, the final equilibrium temperature T_e relates to the initial temperature T_i according to (Hulman et al., 2009):

$$T_e = T_i\left[1 + Q/A\big/\left(2\varepsilon\sigma T_i^4\right)\right]^{1/4} \quad (3)$$

with the emissivity $\varepsilon = 1.0$ for the ideal case of black-body radiation and $Q/A = jE/A$ the energy of the electron beam per surface area in W m^{-2}. Equation (3) shows that the electron flux should not exceed a critical electron flux j_c if we require $T_e < T_c$. We will test this simple assumption in the results section.

3. Experiment set-up

We performed the experiments in the MEFISTO test facility at the University of Bern (see previous studies by Galli et al. (2016, 2017)). The facility consists of a 1.6 m^3-sized vacuum chamber, the ice samples to be irradiated were mounted on a hollow steel plate cooled with liquid nitrogen. The total pressure achieved inside the chamber during the experiments was typically 10^{-8} mbar. We used an electron gun (nominal energy range 100 eV to 10 keV, manufacturer: Kimball Physics) to irradiate the ice samples. The ion source of the MEFISTO facility was used only for a test with the ice slab sample (see next section).

3.1. Sample preparation

For this study, we prepared five different types of water ice samples: a compact ice film on a microbalance ("film"), a thick porous ice sample of fine-grained ice ("fine"), a thick porous ice samples of coarse grains ("coarse"), a thick ice slab ("slab"), and irregular frost on cold metal surfaces ("frost"). The properties of these samples are summarized in Table 1. The column titled "Experiments" indicates the number of successful results with each sample.

The ice film was created by depositing de-ionized water vapour on a microbalance (gold-coated 15 MHz quartz crystal, manufacturer: QCM Research) cooled to 90 K (for a detailed description see Galli et al. (2017)). We controlled the thickness of the layer by recording the frequency of the microbalance and assumed that the ice density is 0.9 g cm^{-3} as in Galli et al. (2017). In said study, we also observed that the ice film thickness must be thicker than the penetration depth of impactors to ensure trustworthy results. Otherwise, the derived sputtering yield can deviate from the actual value by more than a factor of two (cf. Fig. 1 in Galli et al. (2017)).

Table 1
Properties of the five different ice samples prepared for this study.

Type	Thickness	Sample density	Structure	Composition	Experiments
Film	≃0.1μm	0.9 g cm^{-3}	amorphous	H_2O	29
Fine	0.9 cm	0.23 g cm^{-3}	Ih, 4.5-μm grains	H_2O	24
coarse	0.9 cm	0.5 g cm^{-3}	Ih, 67-μm grains	H_2O & NaCl	20
slab	1.0 cm	0.97 g cm^{-3}	Ih	H_2O & NaCl	8
frost	≃0.1 mm	N/A	Ih, irregular	H_2O	6

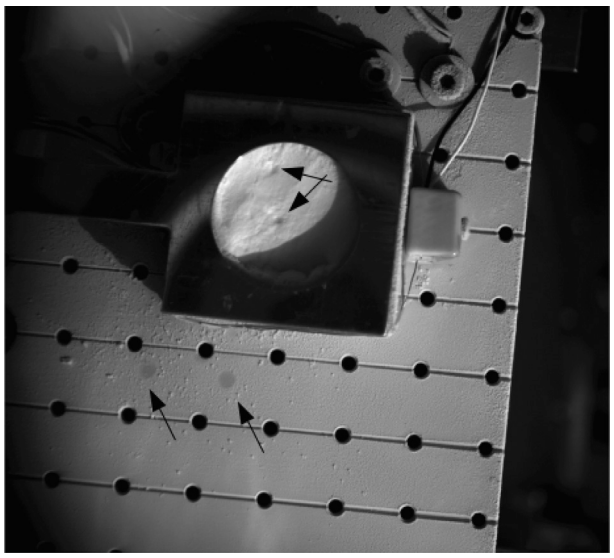

Fig. 1. CCD camera image of the fine-grained ice sample after two days of electron irradiation experiments. The diameter of the circular ice sample is 4 cm. The dark circles in the frost and the depressions inside the ice sample (pointed out by black arrows) indicate ice sublimation caused by intense electron beams.

The fine-grained ice was produced with the same method as described by Galli et al. (2016) and by Jost et al. (2016) using the Setup for the Production of Icy Planetary Analogs: we used an ultrasonic nebulizer to produce micrometer sized droplets (average size = 4.5 μm, macroscopic density = 0.23 g cm^{-3}) of pure de-ionized H_2O. The porous ice was then inserted in the pre-cooled aluminum sample holder (4 cm inner diameter and 0.9 cm depth). A CCD image of the fine-grained ice inside the sample holder during irradiation experiments is shown in Fig. 1. The same sample holder was used for the other series with coarse-grained ice and the ice slab.

The coarse-grained ice was produced with the method described by Yoldi et al. (2015); Poch et al. (2016). A mixture of 99 wt% de-ionized H_2O and 1 wt% NaCl was sprayed into microdroplets by an ultrasonic unit equipped with a sonotrode. The droplets were frozen in liquid nitrogen to form coarse-grained ice particles with an average size = 67±31 μm and a sample density of 0.5 g cm^{-3}. We added NaCl to see if this would be ejected from the sample and to have a more realistic analogue for the surface of Europa. However, we never detected Na or Cl in the mass spectrum of released particles during irradiation, and we could not detect any influence of the salt on electric or thermal properties or on sputtering yield.

At the end of one week of experiments, the surface of the coarse-grained ice sample exhibited a yellowish hue. Hand and Carlson (2011) observed a similar change of colour after having irradiated pure NaCl crystals with 10 keV electrons. The colour change did, however, not appear in the other two weeks of experiments with the coarse-grained ice (nor for any other ice sample). We plan to examine such surface alterations more quantitatively in future studies.

For one measurement week we experimented with a slab of ice. As for the coarse-grained ice, we mixed 99 wt% de-ionized H_2O and 1 wt% NaCl, then let it freeze within a few minutes inside the sample holder at $T = -40$°C. The density was 0.97±0.1 g cm^{-3}.

The irregular frost was a side-effect of our experiment procedure: The thick ice samples had to be created at ambient pressure and cooling must proceed pumping of the chamber to avoid sublimation. As a result, water vapour from the ambient air formed a frost layer on all cool metal surfaces (Galli et al., 2016). For comparison's sake we also irradiated this irregular frost layer with electrons. Moreover, we once removed the frost from the ice slab by sputtering with a 30 keV He^+ ion beam and then checked if the electron sputtering yields had changed.

3.2. Experiment procedure and measurement method

For the microbalance set-up, the measurement procedure was identical to the one described in Galli et al. (2017): after vapour-depositing a water ice film on the microbalance, we chose an electron beam and centered it on the surface of the microbalance by minimizing the frequency of the microbalance. This indicated that the loss rate of water ice was maximized.

Both for the microbalance and the deep ice samples, a copper plate served as Faraday cup to measure the electron flux and the size of the beam. The Faraday cup was operated at a positive potential of 18 V (Galli et al., 2016) and was 2 × 2 cm^2 in size, thus covering the entire electron beam of 0.5–1 cm diameter. Since the active surface area of the microbalance (0.316 cm^2) was smaller or comparable to the electron beam size, we used copper wires (diameter = 0.14 cm) attached to the Faraday cup to measure the electron beam profile at a finer resolution. The ice sample holder of 4 cm diameter, on the other hand, was much larger than the electron beam.

We repeated the ice film irradiations for pristine and previously irradiated ice to assess saturation effects. For this experiment set-up, the sputtering yield can easily be derived from the mass loss rate indicated by the frequency of the microbalance. Nevertheless, we also monitored the pressure in the vacuum chamber with a Stabil-Ion pressure gauge (manufacturer: Granville-Phillips) at intervals of 1 s. This allowed us to relate the sputtering yield to an observed pressure rise. This is necessary to derive sputtering yields from experiments with thick ice samples: ice layers thicker than micrometers cannot be attached on a microbalance and the deposited mass could not be weighed.

The method of deducing sputtering yields from pressure measurements was tested in Galli et al. (2017): The pressure rise Δp appeared with the onset of irradiation and disappeared again when the electron gun was shut down. Δp can be interpreted as the result of a surplus of thermalized sputtering products created by electrons irradiating the ice at a current j (q_e is the elementary charge):

$$Y = c\frac{\Delta p S q_e}{k_B T j} \tag{4}$$

The effective pumping speed of the vacuum chamber $S = 0.25$ m^3 s^{-1} can be deduced from the timescale with which the pressure returns to background levels, the conversion factor c is less than 1 because many of the ejected molecules will not remain in the gas phase but rather stick to the inner surfaces of the vacuum chamber instead. The actual value depends on the geometry of the vacuum chamber and on the vacuum pump (see Galli et al. (2017) for details). We verified the conversion factor again for the new microbalance experiments (see Section 4.1); the accuracy of Equation (4) is roughly 30%.

The experiment set-up for thick ice samples followed the study by (Galli et al., 2016): we inserted the ice samples in the sample holder on the cooling plate and evacuated the vacuum chamber. After pumping is initiated, the pressure takes roughly one day to reach the same level of ≃10^{-8} mbar achieved for the microbalance set-up. The ice sample was normally kept at a constant temperature of roughly 100 K throughout a series of experiments lasting 4 days. We invested 2, 2, 3, and 1 weeks for the ice films, fine-grained ice, coarse-grained ice, and the ice slab. A single irradiation lasted between 2 and 30 min. A copper wire wrapped around the sample holder allowed us to heat the ice to some degree via Ohmic heating (visible in Fig. 1). We made use of that heater once to study temperature effects. Electron irradiation experiments were performed at various impact angles, energies, and electron fluxes. After 4 days, the ice sample was retrieved and discarded. We did not yet analyze the remaining ice in a quantitative way, we monitored only the particles leaving the ice. We plan to use this set-up in the future also to characterize how ice surfaces are altered by long-term irradiation.

A mass spectrometer (HAL quadrupole gas analyser, manufacturer: Hiden Analytical) was mounted to the ceiling of the vacuum chamber, 80 cm above the ice sample. It ran continuously like the pressure gauge. It

was used to analyze the relative chemical composition of released neutrals as its absolute sensitivity was inferior to the Stabil-Ion pressure gauge. Charged ejecta could not be detected with the mass spectrometer.

4. Results and discussion

In total, our measurement series provided us with 40, 24, 20, 8, and 6 useful irradiation experiments for ice films, fine-grained ice, coarse-grained ice, ice slab, and frost, respectively (see Table 1). Useful experiments imply no sublimation effects and derived sputtering yields with a relative accuracy of 50% or better. We first discuss the ice film results as they are required to evaluate the experiments with thick ice samples.

4.1. Microbalance experiments

The temperature of the ice film on the microbalance was 90.0±2.0 K, i.e., similar to the 91–93 K in Galli et al. (2017).

The sputtering yield was found to be constant with time after the very first irradiation of a pristine ice film. For the case of a 0.2 keV electron beam, the water loss from the surface continually increased until it reached a stable rate after 60 s, corresponding to a fluence of roughly 4×10^{14} e^- cm^{-2}. Other experiments with 1, 3, and 5 keV electrons showed a similar time dependence with saturation doses between 10^{14} and 10^{15} e^- cm^{-2}. These values are of the same order of magnitude as the saturation dose of 2×10^{15} e^- cm^{-2} found by Orlando and Sieger (2003) for the release of O^2 due to 100 eV electrons irradiating water ice films at 120 K.

Table 2 summarizes the sputtering yields Y_{H_2O} (in terms of water lost from the microbalance) measured at various electron energies for saturated water ice films. The yield corresponds to the total loss of water molecules from the microbalance. The uncertainty of sputtering yield of 1/3 is introduced by the fluctuating current of the electron gun at the required low intensities and by other factors such as saturation effects and varying ice film thickness. This uncertainty is comparable to the uncertainty of previous sputtering experiments at low electron energies (±50% according to Teolis et al. (2010)). For energies from 0.2 to 1.0 keV, all sputtering yields cluster around $Y = 2.0 \pm 0.5$ and the dependence on impact angle θ is small; the only exception to this rule is the case of 0.5 keV. We multiplied $Y_{O_2}(E, T, \theta)$ by a factor of two to compare the results with predictions in Table 2. The underlying assumption was that two water molecules in the ice film underwent radiolysis to create one O^2 molecule.

The predicted yield $2Y_{O_2}(E, T, \theta)$ from Equation (1) agrees well with the observed yield of 2.0 in the energy range from 0.2 to 1 keV. On the other hand, the measured yield does not significantly decrease above 1 keV; it remains constant within error bars between 0.7 and 3 keV for 45° impact angle (see Table 2). We tried to expand the energy range by irradiating the microbalance with 5 keV electrons. The reproducibility of these data, however, turned out to be not better than a factor of 3 when we repeated these measurements several times for varying electron beam intensities and ice film thicknesses. Our conjecture is that the ice film thickness is no longer sufficiently thick compared to the penetration depth of electrons at 5 keV (550 nm for $\theta = 45°$). The maximum thickness for which a linear behaviour of frequency with mass deposition rate can be assumed corresponds to a few 100 nm only. The yield of energetic electrons will have to be addressed again in the section on thick ice samples (Section 4.2).

The pressure in the vacuum chamber (measured with the Stabil-Ion pressure gauge) increased at the onset of irradiation to a higher plateau and returned to the background level with an exponential decay time of 6.5±1.5 s when the electron gun was shut down. The same decay time was found when we irradiated thick ice films with electrons. The mass spectrometer detected only H_2 and minor contributions of O and O_2 to rise and fall with the start and stop of electron irradiation. The partial pressure of H_2O did not notably increase during the experiments so long as the ice film was much thicker than the penetration depth of electrons. We thus assume, as in Galli et al. (2017) that every H_2O molecule lost from the microbalance is converted into $H_2 + 1/2\ O_2$.

With this information, we can predict the pressure rise caused by sputtering (Equation (4)) and compare it with the measurement of the Stabil-Ion pressure gauge. We rely on this pressure gauge for changes in total pressure because it is more sensitive and accurate than the mass spectrometer. From the previous sputtering study (Galli et al., 2017) we expect a constant ratio between predicted and measured total pressure.

Fig. 2 shows the measured versus the predicted total pressure from Equation (4) with $S = 0.25$ m^3 s^{-1} for all microbalance experiments with electron energies from 0.2 to 2.0 keV, i.e., excluding those for which the ice film certainly was not thick enough. The conversion factor c is 0.11±0.025, the error bar being dominated by the uncertainty of the pumping speed. For this specific experiment set-up and pressure range, c does not notably change if the major gas species is H_2O or a non-watery species (see Fig. 5 in Galli et al. (2017).

Having derived the conversion factor between predicted and actually measured pressure rise, we can convert the measured pressure rises from irradiation of thick ice layers into absolute sputtering yields. The height of the pressure rise (few 10^{-10} to few 10^{-9} mbar) is comparable for both experiment set-ups.

4.2. Experiments with thick ice samples

The results in terms of total sputtering yield and chemical composition are similar for all four different thick ice targets (ice slab, fine-grained regolith, coarse-grained regolith, and frost). Therefore, we

Table 2
Measured (Y) and predicted (Y_p) electron sputtering yields for water equivalent mass loss per incident electron. θ denotes the impact angle relative to the surface normal, d is the ice film thickness, $d_p\cos(\theta)$ is the expected penetration depth according to Equation (2).

Energy (keV)	θ (°)	$Y \pm \sigma_Y$	d (nm)	Y_p	$d_p\cos(\theta)$ (nm)
0.2	30°	2.0±0.6	28	1.95	2.3
0.2	45°	2.0±0.6	30	2.09	1.9
0.4	30°	2.3±0.7	28	1.91	7.8
0.4	45°	2.4±0.8	30	2.24	6.4
0.5	30°	2.4±0.8	77	1.69	12
0.5	45°	3.3±1.0	85	2.03	9.9
0.7	30°	1.8±0.6	72	1.33	22
0.7	45°	1.9±0.6	110	1.62	18
1.0	45°	1.9±0.6	117	1.24	33
2.0	30°	0.8±0.2	174	0.60	135
2.0	45°	1.4±0.3	196	0.73	110
2.0	60°	2.2±0.7	183	1.03	78
3.0	45°	$1.6^{+0.2}_{-0.6}$	162	0.54	225

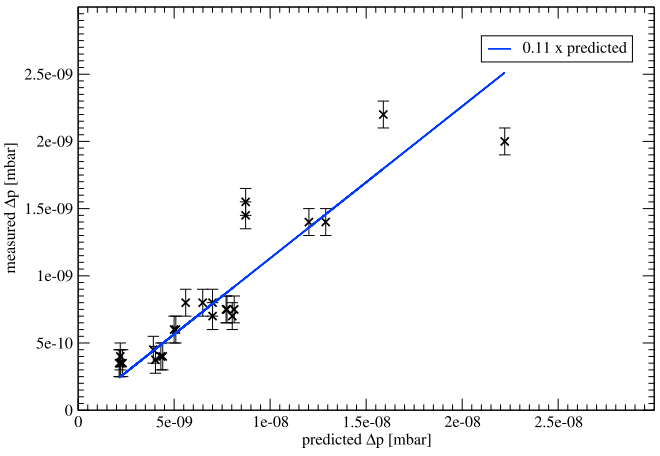

Fig. 2. Measured versus predicted pressure rise for irradiation experiments of water ice films.

collect all these results in one common section. The temperatures of the ice samples varied slightly between different irradiation experiments around $T = 98\pm2$K.

Contrary to the microbalance experiments, the ice thickness of 0.9 cm always exceeds the electron penetration depth by orders of magnitude. On the other hand, the surface of a thick ice sample is electrically and thermically discoupled from the cooling plate. This can, in principle, lead to two experimental problems when the ice surface is irradiated with charged particles. The surface can charge up to a potential that disturbs the electron beam and the surface can heat up to such a degree that the surface ice starts sublimating. The first problem never occurred, the second did.

The assumption that the secondary electron yield exceeds unity (see Section 2) for our electron energies agrees with observations: the observed pressure and thus the release rate from the ice remained stable throughout electron irradiation of any duration (2–30 min). If the surface had charged up to a negative potential, the sputtering yield would have decreased with time while the current measured with the ring-shaped Faraday cup around the ice sample would have increased. This was not observed during electron irradiation, but both effects were observed when we irradiated similar ice samples with energetic ion beams (Galli et al., 2016).

The most obvious indication for sublimation is the occurrence of holes and depressions in the ice sample upon electron irradiation. This is demonstrated in Fig. 1. This CCD camera image shows the sample of fine-grained ice on the cooling plate at the end of electron irradiation. The two dark circles on the cooling plate of 4.2 mm diameter were created by 2 keV electron beams at 12 μA. The electron beam sublimated the upper frost layers resulting in the dark circles. The same electron beam produced the two depressions inside the ice sample (see arrows in Fig. 1).

We wished to quantify sputtering yields of radiolysis products at a given temperature without sublimation or any other thermal processes. When electron irradiation warmed up the surface to a temperature much higher than the nominal 98 K, the yield of O_2 and H_2 was found to increase. A further increase of the beam intensity then resulted in a clear H_2O signal in the chamber, i.e., ice started sublimating. The pressure rise resulted in a sputtering yield 1–4 times higher than for experiments without sublimation and the abundance of H_2O dominated over H_2. The sublimation limit is expected for 145 K at a saturation pressure of 10^{-8} mbar (Andreas, 2007). To derive sputter yields at a given ice temperature we must not only exclude these sublimation cases but also the intermediate cases of enhanced O_2 and H_2 without sublimation.

We categorized experiments as affected by thermal effects if we recognized a rise of H_2O in the spectrum, if the beam created a depression in the ice surface, if the pressure decreased slowly ($\gg$ 10 s) after electron irradiation had been stopped, or if the drop of partial pressure of H_2 at the end of irradiation exceeded its rise at the onset of irradiation. As a result of this categorization, we found the threshold beam intensities for thermal effects j_c in Table 3. The difference in j_c for fine-grained versus coarse-grained ice was nowhere larger than a factor of two. For energies below 1 keV, sublimation never occurred for any beam intensity up to several μA (at a beam diameter of 6 mm). According to Equation (3) the final temperature of the ice surface irradiated with j_c reached 237 K both for 3 and 10 keV. Equation (3) probably overestimates the temperature. The reason for this overestimation is that beside radiation, heat conduction still lowers the temperature even on short timescales of seconds to minutes.

Table 3
Threshold beam intensity j_c above which ice starts sublimating. The surface ice temperature before irradiation was 98±2 K and the electron impact angle was $\theta = 45°$.

Energy (keV)	j_c (μA)
3.0	2.5±0.5
10.0	0.8±0.2

Unless otherwise stated, only experiments without thermal contributions are discussed in this section. We verified that for this subset of data the derived sputter yield does not depend on electron intensity. For instance, two experiments with 10 keV electrons irradiating coarse grained ice resulted in $Y = 8.1\pm2.7$, 8.5 ± 2.7 for $j = 0.14$ and 0.86 μA. For 0.7 keV, a constant yield was observed for electron currents from 0.4 to 5 μA.

When a pristine part of the ice sample was irradiated with 1–10 keV electrons, H_2 (mass 2 u) partial pressures in the chamber rose immediately. O_2 (mass 32 u), on the other hand, increased from background levels to a stable level within several minutes of irradiation. The abundance of mass 34 u (H_2O_2 and $^{18}O^{16}O$) followed in most cases the temporal evolution of O_2; a deviation with time between masses 34 and 32 was observed once when the ice sample was heated after irradiation. In 5 different cases with 1, 2, 5, and 10 keV of an irradiation of fine-grained ice that was either pristine or had not been irradiated for several hours, the saturation times corresponded to an electron deposition of 1×10^{16} e^- cm^{-2} for 1 and 2 keV and $2\pm1 \times 10^{16}$ e^- cm^{-2} for 5 and 10 keV. For a low electron energy of 0.2 keV, the saturation dose was 10^{14} to 10^{15} e^- cm^{-2} as for the microbalance experiments, which had shown a similar increase of mass loss rate during the first few minutes of irradiation (see Section 4.1). The experiments with other ice targets featured insufficient pressure rises to properly discern saturation timescales. Hand and Carlson (2011) reached equilibrium concentrations only at a fluence of 10^{19} eV cm^{-2} when they studied absorption features of the H_2O_2 building up in ice films irradiated with 10 keV electrons.

Fig. 3 illustrates saturation and sublimation effects. It tracks the temporal evolution of the partial pressures of H_2O (blue), O_2 (green), H_2 (orange), and mass 34 (black, lower panel) for a sequence of four irradiations on the same spot of fine-grained ice. The onset of electron irradiation is indicated with red dotted lines, shutdown is indicated with dashed-dotted lines. The sequence of irradiation for the example in Fig. 3 was 1 keV electrons with 5×10^{13} e^- cm^{-2} s^{-1}, a stronger 1 keV beam with 9×10^{13} e^- cm^{-2} s^{-1}, followed by a weak (2×10^{13} e^- cm^{-2} s^{-1}) and an intense (9×10^{13} e^- cm^{-2} s^{-1}) 10 keV beam. The latter was so intense as to trigger sublimation; the H_2O partial pressure kept increasing during several minutes after irradiation had begun. Such experiments were excluded from further analysis. During the first irradiation experiment in Fig. 3, O_2 reached a similar level above background as the H_2 increase after 3±2 minutes, corresponding to the saturation fluence of 10^{16} e^- cm^{-2}. The temporal resolution of the mass spectrometer was 8 s.

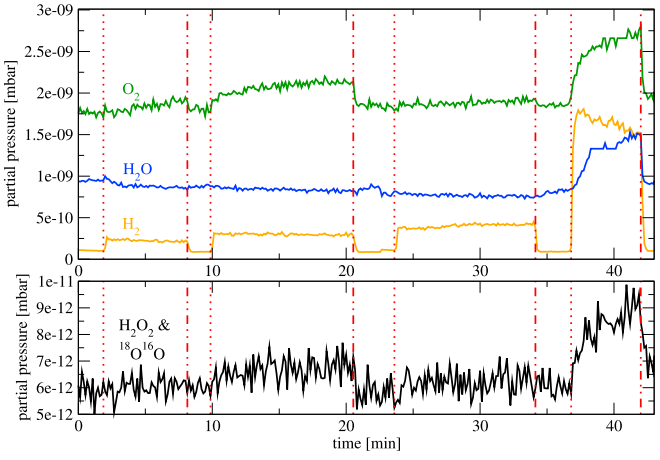

Fig. 3. Timeseries of H_2O (blue), O_2 (green), H_2 (orange), and H_2O_2 & $^{18}O^{16}O$ (black, lower panel) for a sequence of four irradiations on the same spot of fine-grained ice. Y-axes indicate the partial pressures in mbar, x-axis is the experiment time in minutes, the red dotted and dashed-dotted lines indicate the onset and end of electron irradiations. (For interpretation of the references to colour in this figure legend, the reader is referred to the web version of this article.)

H_2 and O_2 were the only species consistently showing a higher partial pressure during irradiation compared to the background before and after irradiation. Taking into account all saturated mass spectra with a sufficient signal-to-noise ratio and without thermal effects, the average ratio of H_2/O_2 was found to vary within 2±1. This average includes 16 different irradiation experiments with fine-grained ice and frost and electron energies ranging from 0.4 to 10 keV. The relative mass abundances (Table 4) did not vary with electron energy, impact angle ($\theta = 30°…60°$), or ice properties (frost or fine-grained ice). Even for high energies with penetration depths of micrometers, it was only a matter of few minutes until all radiolysis products started leaving the ice. This means, on the other hand, that after an irradiation stop of several hours, O_2 had to be built up anew when irradiation recommenced. No H_2O above the detection limit (10% of total pressure rise) was released for any energy and electron flux so long as the latter remained below j_c. Recently, Abdulgalil et al. (2017) also observed that H_2 and O_2 were the major gas-phase products from desorption, rather than intact H_2O, when they irradiated amorphous water ice films of 100 K with 200–300 eV electrons.

H_2O_2 was probably detected when the total pressure rise was sufficiently large: The observed H_2O_2 signal must be corrected because the resolution of the mass spectrometer at 34 u is insufficient to discriminate between $^{18}O^{16}O$ and H_2O_2. Assuming a relative abundance of 0.00205 for the ^{18}O isotope (Rosman and Taylor, 1999), 12 of the 16 experiments show an H_2O_2 signal above the detection limit; the average and standard deviation over all 16 experiments calculate to an H_2O_2 abundance of 0.001±0.001 of the total pressure rise. The abundance of the presumed H_2O_2 did not depend on energy or impact angle either. Table 4 summarizes these findings.

The temporal dependence and the H_2/O_2 ratio are consistent with the expectation that water molecules are radiolysed into H_2 and O_2 and to a small fraction of H_2O_2 (see Section 2). The H_2 leaves the ice sample immediately (within the few seconds of temporal resolution provided by the mass spectrometer), whereas the produced O_2 and H_2O_2 must reach a certain concentration before they are released as well.

The range of 0.1±0.1% H_2O_2 abundance agrees well with the observed molar concentration on Europa's surface of 0.13% (Carlson et al., 1999). Loeffler et al. (2006) measured equilibrium concentrations of 0.14% and 0.1% for irradiation with 100 keV H^+ at 80 K and 120 K; Hand and Carlson (2011) found an equilibrium molar H_2O_2 concentration of 0.029% relative to water inside the ice films they had irradiated with 10 keV electrons. Teolis et al. (2017) predicted that the bulk abundance of H_2O_2 created by electron radiolysis should exceed the abundance near the ice surface; we could not test this prediction because we could not measure bulk abundances of our ice samples after irradiation. But our results imply that electrons with energies on the order of 1 keV can also produce the observed fraction of H_2O_2 in Europa's surface. The H_2O_2 can then trigger further chemical reactions in the ice.

Other species like H, O, OH, H_3O may be produced in water ice, too (Johnson and Quickenden, 1997). But in our experiments their abundances mostly varied with the abundance of H_2O in the chamber, independent of electron irradiation. H_2O can fragment into OH and H when it is ionized in the mass spectrometer. For irradiation experiments without H_2O increase, no clear rise in OH and H_3O was ever observed. This translates into an upper limit of 5% volume ratio each for OH and H_3O during our experiments.

Table 4
Relative abundances of released gas species during electron irradiation, averaged over 16 different irradiation experiments with fine-grained-ice and frost for electron energies between 0.4 and 10 keV.

Species	relative abundance
H_2	0.66±0.16
O_2	0.33±0.17
H_2O_2	0.001±0.001
H_2O	<0.10

From the energy-independent chemical composition of the ejecta it should come as no surprise that the absolute sputtering yield does not vary significantly with electron energies once radiolysis in the ice has reached saturation. Table 5 shows all available sputtering yields, i.e., number of water molecules lost from the ice per impacting electron. The error bar of a single Y value in that table amounts to 33%: the uncertainty of the conversion factor (Fig. 2) is 25% and the uncertainty of the electron flux hitting the ice surface is 10–20%. No universal effect of the impact angle on sputtering yields can be seen. In the following we will therefore concentrate on the observations at $\theta = 45°$ and compare them to the prediction in Equation (1) and to the sputtering yields caused by ions.

Fig. 4 shows the sputtering yield $Y_{H_2O}(E)$ in ratio of water molecules destroyed or lost from the ice per impactor. The other Fig. 5 shows $Y_{O_2}(E)$. For the observations, this is just half of the $Y_{H_2O}(E)$ (see the chemical composition in Table 4). The data points in Figs. 4 and 5 are those values in Tables 2 and 5 measured at $\theta = 45°$. The microbalance results from Table 2 and from the previous publication (Galli et al., 2017) were scaled to 98 K as well, assuming the temperature dependence in Equation (1). The theoretical curves in Fig. 4 for ion (green solid) and electron (red dashed) sputtering were calculated for $\theta = 45°$ and $T = 98$ K. The magenta curve in Fig. 5 shows the O_2 yield for oxygen ions of the same energy impacting ice regolith (Teolis et al., 2010). We assumed that the angular average the authors calculated for their $Y_{O_2}(E)$ should be representative to the $\theta = 45°$ impact angle in our experiments.

We warmed up the fine-grained ice sample at the end of a measurement week to check for temperature effects. Heating the wire around the sample holder sublimated a lot of frost, which led to a large transient pressure rise in H_2O. After waiting 2 h while keeping the heat current stable, we managed to repeat irradiation experiments with 1 and 10 keV electrons at an acceptable background pressure and $T = 108$ K instead of the usual 98 K. Neither the timescales for saturation, nor the chemical composition of ejecta, nor the absolute yield changed in a noticeable manner compared to the cooler case. Equation (1) predicts a relative increase of 1.46 in sputtering yield at this higher temperature. The measured Y_{H_2O} for 1 keV was 3.5, thus within the range of sputtering

Table 5
Electron sputtering yields once an ice target reached saturation: Y is the ratio of removed H_2O molecules (most of them as H_2 and O_2) per impacting electron.

Y	Energy (keV)	Ice type	Impact angle θ
3.0	0.5	coarse	45
3.7	1.0	coarse	45
4.3	3.0	coarse	30
4.1	3.0	coarse	45
3.1	3.0	coarse	60
4–8	10	coarse	30
4–11	10	coarse	45
4.5	0.2	fine	45
4.9	0.4	fine	45
5.3	0.5	fine	32
4.4	0.5	fine	45
5.0	0.5	fine	58
4.0	0.7	fine	45
2.0–4.4	1.0	fine	45
2.8	2.0	fine	32
3.2	2.0	fine	45
4.1	2.0	fine	58
5.6	5.0	fine	32
5.0	5.0	fine	45
3.6	0.5	frost	45
3.4	0.7	frost	45
4.0	1.0	frost	30
5.6	3.0	frost	60
5.6	10	frost	45
2.0	1.0	slab	30
3.4	1.0	slab	45
2.5	3.0	slab	60
4.0	10	slab	30
5–11	10	slab	45

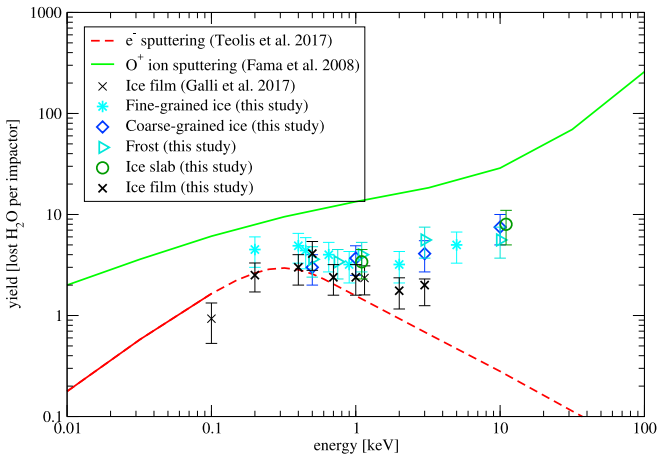

Fig. 4. Theoretical and observed sputtering yields in equivalent water molecules lost per impactor for an impact angle of 45° and an ice temperature of 98 K. The solid curves are semi-empirical formulae based on previously existing experiments, the red dashed curve is a theoretical extrapolation (Teolis et al., 2017). The symbols show all experiment results obtained at $\theta = 45°$ in the present study and from Galli et al. (2017). (For interpretation of the references to colour in this figure legend, the reader is referred to the web version of this article.)

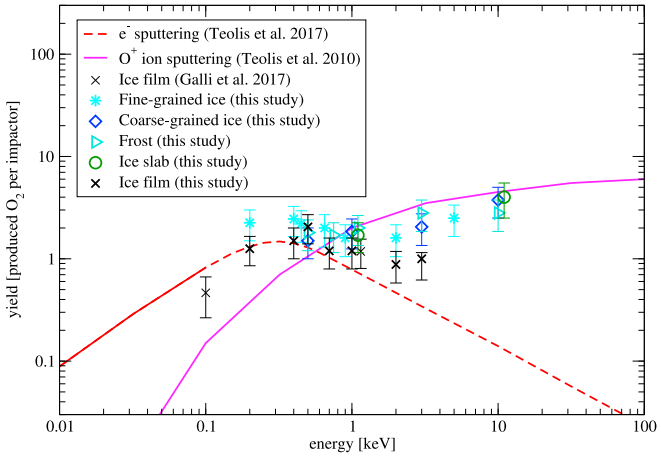

Fig. 5. Theoretical and observed sputtering yields in equivalents of produced O_2 molecules per impactor. Same format as Fig. 4.

yields at lower temperatures. For 10 keV, $Y_{H_2O} = 11$ was higher, but not significantly higher, than for irradiation experiments with other ice samples at colder temperature. Probably, the achievable temperature rise was insufficient to see a significant increase of yields as their relative uncertainty of 1/3 is comparable to the expected increase.

The physical properties of the ice sample have no significant effect on sputtering yields. For energies where sufficient ice film thicknesses are possible, the microbalance results agree with the thick samples. Comparing Y (scaled to 98 K) from ice films to fine-grained ice at the same energies and impact angles, we observe a ratio of $Y_{film}/Y_{fine} = 0.71 \pm 0.2$. The yield from deep, porous targets is larger or as large as the one from ice films. Apparently, Equation (1) can be applied both to compact and porous ice targets provided the scale of porosity (5 or 70 μm in our case) is much larger than the 2.8 nm surface layer relevant for O_2 production (Teolis et al., 2017). The removal of the frost layer on the ice slab with a 30 keV He^+ beam did not change the sputtering yield measured with 10 keV electrons before and after ion irradiation.

For energies up to 1 keV, the predictions match the measurements. The yields then seem to reach a local minimum at 1–2 keV, but this drop is not significant given the error bars. On the other hand, the yields clearly do not decrease with energy from 3 to 10 keV, contrary to Equation (1) (compare red curve with data points in Fig. 4). In terms of water loss the yield caused by electrons is still much smaller than the erosion caused by oxygen ions of comparable energy (green curve in Fig. 4). On the other hand, we note in Fig. 5 that electrons between 3 and 10 keV release a similar amount of O_2 as O^+ ions do.

Two explanations for the discrepancy between predictions and measurements above 2 keV are possible. Equation (1) may be correct, but the ice is damaged by electron irradiation in such a way that eventually all products are released no matter at which depth in the ice radiolysis occurred. Since an energetic electron will proceed in the ice until it has deposited its entire energy, one could integrate Equation (1) from the initial electron energy to the lower limit of radiolysis (10 eV (Orlando and Sieger, 2003; Teolis et al., 2010)). Alternatively, we would have to postulate an additional loss process becoming relevant for energies above a few keV, such as secondary electrons being released inside the ice while the primary electrons are losing their energy.

5. Conclusions

- We have presented the first experimental sputtering yields for energetic electrons between 0.2 and 10 keV irradiating water ice. We used two different measurement methods, eroding ice films from a microbalance or measuring the pressure rise caused by the release of particles into the vacuum chamber.
- The results do not depend on physical properties (grain-size and porosity) of the ice within the 33% uncertainty of measured sputtering yields.
- As found in previous irradiation experiments, most H_2O molecules are radiolysed into H_2 + 1/2 O_2. H_2O_2 was probably detected, too, at a relative abundance of 0.001±0.001. This fraction agrees well with derived H_2O_2 concentrations on Europa's surface.
- The predictions for the absolute yield of O_2 production and H_2O destruction based on previous experiments at energies below 0.1 keV have been confirmed for electron energies up to 1 keV. On the other hand, the measured yield at energies from 3 to 10 keV does not decrease compared to the yield around 0.5 keV. The O_2 yield thus is considerably higher than expected for these energies and is of similar importance for the O_2 production as O^+ ions of the same energy.
- It was clear before this study that electron irradiation is important for energy deposition in deeper layers and chemical alterations of the surfaces of icy moons. Now it seems that electrons are relevant as well for the creation of oxygen-rich atmospheres around icy moons such as Europa and Ganymede.

Acknowledgements

The work in this paper has been partially performed in the context of the activities of the ISSI International Team Nr. 322, www.issibern.ch/teams/exospherejuice/. We also would like to thank G. Bodmer, J. Gonseth, and A. Etter for their relentless support of the scientific work at the MEFISTO facility.

References

Abdulgalil, A.G.M., Rosu-Finsen, A., Marchione, D., Thrower, J.D., Collings, M.P., McCoustra, M.R.S., 2017. Electron-promoted desorption from water ice surfaces: neutral gas- phase products. ACS Earth Space Chem. 1, 209–215.
Andreas, E.L., 2007. New estimates for the sublimation rate for ice on the Moon. Icarus 186, 24–30.
Baragiola, R.A., Atteberry, C.L., Dukes, C.A., Famá, M., Teolis, B.D., 2002. Atomic collisions in solids: astronomical applications. Nucl. Instrum. Methods Phys. Res. B 193, 720–726.
Baragiola, R.A., Fama, M., Loeffler, M.J., Raut, U., Shi, J., 2008. Radiation effects in ice: new results. Nucl. Instrum. Methods Phys. Res. B 266, 3057–3062.
Boring, J.W., Johnson, R.E., Reimann, C.T., Garret, J.W., Brown, W.L., Marcantonio, K.J., 1983. Ion-induced chemistry in condensed gas solids. Nucl. Instrum. Methods Phys. Res. 218, 707–711.

Carlson, R.W., Anderson, M.S., Johnson, R.E., Smythe, W.D., Hendrix, A.R., Barth, C.A., Soderblom, L.A., Hansen, G.B., McCord, T.B., Dalton, J.B., Clark, R.N., Shirley, J.H., Ocampo, A.C., Matson, D.L., 1999. Hydrogen peroxide on the surface of Europa. Science 283, 2062–2064.

Cassidy, T.A., Paranicas, C.P., Shirley, J.H., Dalton III, J.B., Teolis, B.D., Johnson, R.E., Kamp, L., Hendrix, A.R., 2013. Magnetospheric ion sputtering and water ice grain size at Europa. Planet. Space Sci. 77, 64–73.

Famá, M., Shi, J., Baragiola, R.A., 2008. Sputtering of ice by low-energy ions. Surf. Sci. 602, 156.

Galli, A., Vorburger, A., Pommerol, A., Wurz, P., Jost, B., Poch, O., Brouet, Y., Tulej, M., Thomas, N., 2016. Surface charging of thick porous water ice layers relevant for ion sputtering experiments. Planet. Space Sci. 126, 6371.

Galli, A., Vorburger, A., Wurz, P., Tulej, M., 2017. Sputtering of water ice films: a re-assessment with singly and doubly charged oxygen and argon ions, molecular oxygen, and electrons. Icarus 291, 36–45.

Hand, K.P., Carlson, R.W., 2011. H_2O_2 production by high-energy electrons on icy satellites as a function of surface temperature and electron flux. Icarus 215, 226–233.

Haring, R.A., Pedrys, R., Oostra, D.J., Haring, A., De Vries, A.E., 1984. Reactive sputtering of simple condensed gases by keV ions III: kinetic energy distributions. Nucl. Instrum. Methods Phys. Res. B5, 483–488.

Hulman, M., Skákalová, V., Krasheninnikov, A.V., Roth, S., 2009. Effects of ion beam heating on Raman spectra of single-walled carbon nanotubes. Appl. Phys. Lett. 94, 071907.

Johnson, R.E., 1990. Energetic Charged-particle Interactions with Atmospheres and Surfaces. Springer-Verlag, New York.

Johnson, R.E., Quickenden, T.I., 1997. Photolysis and radiolysis of water ice on outer Solar System bodies. J. Geophys. Res. 102, 10985–10996.

Johnson, R.E., Carlson, R.W., Cooper, J.F., Paranicas, C., Moore, M.H., Wong, M.C., 2004. Radiation effects on the surfaces of the Galilean satellites. In: Bagenal, F. (Ed.), Jupiter: Atmosphere, Satellites and Magnetosphere. University of Arizona Press, Tucson, USA.

Johnson, R.E., Carlson, R.W., Cassidy, T.A., Famá, M., 2013. Sputtering of ices. In: Gudipati, M.S., Castillo-Rogez, J. (Eds.), The Science of Solar System Ices. Springer, New York.

Jost, B., Pommerol, A., Poch, O., Gundlach, B., Leboeuf, M., Dadras, M., Blum, J., Thomas, N., 2016. Experimental characterization of the opposition surge in fine-grained water-ice and high albedo analogs. Icarus 264, 109–131.

Jurac, S., Baragiola, R.A., Johnson, R.E., Sittler Jr., E.C., 1995. Charging of ice grains by low-energy plasmas: application to Saturn's *E* ring. J. Geophys. Res. 100 (A8), 14821–14831.

Loeffler, M.J., Raut, U., Vidal, R.A., Baragiola, R.A., Carlson, R.W., 2006. Synthesis of hydrogen peroxide in water ice by ion irradiation. Icarus 180, 265–273.

Muntean, E.A., Lacerda, P., Field, T.A., Fitzsimmons, A., Fraser, W.C., Hunniford, A.C., McCullough, R.W., 2016. A laboratory study of water ice erosion by low-energy ions. Mon. Not. R. Astron. Soc. 462, 3361–3367.

Orlando, T.M., Sieger, M.T., 2003. The role of electron-stimulated production of O_2 from water ice in the radiation processing of outer solar system surfaces. Surf. Sci. 528, 1.

Paranicas, C., Carlson, R.W., Johnson, R.E., 2001. Electron bombardment of Europa. Geophys. Res. Lett. 28, 673–676.

Paranicas, C., Mauk, B.H., Ratliff, J.M., Cohen, C., Johnson, R.E., 2002. The ion environment near Europa and its role in surface energetics. Geophys. Res. Lett. 29, 18.

Poch, O., Pommerol, A., Jost, B., Carrasco, N., Szopa, C., Thomas, N., 2016. Sublimation of water ice mixed with silicates and tholins: evolution of surface texture and reflectance spectra, with implications for comets. Icarus 267, 154–173.

Reimann, C.T., Boring, J.W., Johnson, R.E., Garrett, J.W., Farmer, K.R., 1984. Ion-induced molecular ejection from D_2O ice. Surf. Sci. 147, 227–240.

Rosman, K.J.R., Taylor, P.D.P., 1999. 1997 report of the IUPAC Subcommittee for isotopic abundance measurements. Pure Appl. Chem. 71, 1593–1607.

Shi, J., Famá, M., Teolis, B.D., Baragiola, R.A., 2012. Ion-induced electrostatic charging of ice at 15–160 K. Phys. Rev. B 85, 035424.

Teolis, B.D., Shi, J., Baragiola, R.A., 2009. Formation, trapping, and ejection of radiolytic O_2 from ion-irradiated water ice studied by sputter depth profiling. J. Chem. Phys. 130, 134704.

Teolis, B.D., Jones, G.H., Miles, P.F., Tokar, R.L., Magee, B.A., Waite, J.H., Roussos, E., Young, D.T., Crary, F.J., Coates, A.J., Johnson, R.E., Tseng, W.-L., Baragiola, R.A., 2010. Cassini finds an oxygen–carbon dioxide atmosphere at Saturns icy moon Rhea (Supporting Online Material). Science 330, 1813.

Teolis, B.D., Plainaki, C., Cassidy, T.A., Raut, U., 2017. Quantification of O2, H2, and H2O2 Radiolysis from ice for any Projectile Species, Energy or Temperature: application to Icy Satellites. Submitted to JGR Planets.

Yoldi, Z., Pommerol, A., Jost, B., Poch, O., Gouman, J., Thomas, N., 2015. VIS-NIR reflectance of water ice/regolith analogue mixtures and implications for the detectability of ice mixed within planetary regoliths. Geophys. Res. Lett. 42, 6205–6212.